

# Drug Design Based on the Carbon/Silicon Switch Strategy

Reinhold Tacke and Steffen Dörrich

**Abstract** Silicon chemistry has been demonstrated to be a novel source of chemical diversity in drug design. The carbon/silicon switch strategy, i.e., the strategic replacement of a carbon atom with a silicon atom (sila-substitution) within a well-known drug, with the rest of the molecule being identical, is one of the methods that are currently used for the design and development of new silicon-based drugs. Some of the fundamental differences between carbon and silicon (e.g., differences in the covalent radii and electronegativities) can lead to marked alterations in the physicochemical and biological properties of the sila-drugs. In general, the sila-analogues share the same mode of action as the parent carbon compounds but may have altered biological properties. Incorporation of silicon into a drug can affect and, ideally, improve the pharmacological potency and selectivity, the pharmacodynamics, and the pharmacokinetics. Examples resulting from the carbon/silicon switch strategy are sila-venlafaxine, sila-haloperidol, and disila-bexarotene, the silicon analogues of the serotonin/noradrenaline reuptake inhibitor venlafaxine, the dopamine antagonist haloperidol, and the retinoid agonist bexarotene, respectively. Using these particular examples, the basic principles of the carbon/silicon strategy in drug design are illustrated in this review.

**Keywords** Bexarotene, Bioisosterism, Carbon/silicon switch, Drug design, Haloperidol, Sila-drugs, Silicon, Synthesis and SAR, Venlafaxine

---

R. Tacke (✉) and S. Dörrich  
Institute of Inorganic Chemistry, University of Würzburg, Am Hubland, 97074 Würzburg,  
Germany  
e-mail: [r.tacke@uni-wuerzburg.de](mailto:r.tacke@uni-wuerzburg.de)

## Contents

1	Introduction .....	30
2	Sila-Substitution of Drugs: The Concept .....	31
3	Sila-Substitution of Drugs: Selected Examples .....	32
3.1	Sila-Venlafaxine: A Silicon Analogue of the Serotonin/Noradrenaline Reuptake Inhibitor Venlafaxine .....	32
3.2	Sila-Haloperidol: A Silicon Analogue of the Dopamine Antagonist Haloperidol ...	37
3.3	Disila-Bexarotene: A Silicon Analogue of the Retinoid Agonist Bexarotene .....	45
3.4	Structures of Other Sila-Drugs .....	53
4	Appendix: Sila-Substitution of Odorants .....	55
5	Summary and Outlook .....	56
	References .....	57

## 1 Introduction

Over the past five decades, many biologically active organosilicon compounds have been synthesized, and silicon chemistry has been demonstrated to be a novel source of chemical diversity in drug design (for reviews, see [1–17]). There are two different approaches that can be used for the design of silicon-based drugs: (1) synthesizing a silicon analogue of a known drug in which at least one carbon atom has been replaced by a silicon atom, with the rest of the molecule being identical (carbon/silicon exchange, carbon/silicon switch, sila-substitution) and (2) synthesizing completely new silicon-based classes of compounds (the carbon analogues of which are unknown or do not exist for principal reasons) that exploit specific features of silicon chemistry to address a well-validated target. This contribution is focused exclusively on the first approach, the carbon/silicon switch strategy. The second approach is discussed in [18] of this book.

Almost 50 years ago, Fessenden et al. reported on the first silicon analogues of known organic drugs [19–22]. Following this pioneering work, many sila-drugs have been synthesized and pharmacologically characterized over the past five decades, and nowadays the carbon/silicon switch strategy is an established method in drug design, not only in academia but also in pharmaceutical industry.

As there are many reviews dealing with the carbon/silicon switch strategy, this contribution has not been written as another, updated overview. Instead, this article is focused on the discussion of a few selected examples of this approach to demonstrate the strategic background and to highlight the huge potential of the carbon/silicon switch strategy for drug design. The examples chosen are selected studies of our group and refer to sila-venlafaxine (**1b**), sila-haloperidol (**2b**), and disila-bexarotene (**3b**) and derivatives. These compounds are silicon analogues of the serotonin/noradrenaline reuptake inhibitor venlafaxine (**1a**), the dopamine antagonist haloperidol (**2a**), and the retinoid agonist bexarotene (**3a**), respectively. The chemical structures of the C/Si pairs **1a/1b**, **2a/2b**, and **3a/3b** are shown in Fig. 1.

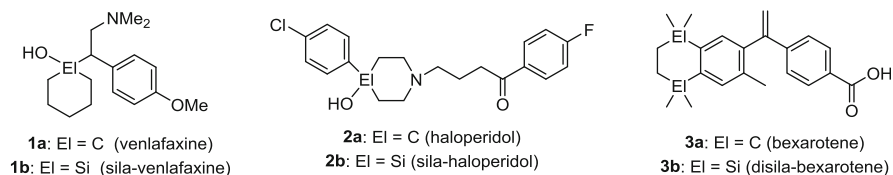


**Fig. 1** Chemical structures of the C/Si pairs **1a/1b–3a/3b**

## 2 Sila-Substitution of Drugs: The Concept

Silicon is similar to carbon in that it forms four covalent bonds with many other elements. Like carbon, silicon is a Group 14 element, possessing many similarities to carbon but also presenting some crucial differences. The following are some of the fundamental differences that can be used to provide a benefit in drug design by using the carbon/silicon switch strategy [1, 4, 8–12, 14, 15, 17].

Silicon (1.17 Å) has a larger covalent radius than carbon (0.77 Å), resulting in the formation of longer silicon–element bonds compared with the analogous carbon–element bonds. For example, the average C–C bond length is 1.54 Å, whereas the Si–C bond length is 1.87 Å. This increase in bond lengths leads to an increase in the size and conformational flexibility of the sila-analogue and also affects its shape. These subtle changes in size, shape, and conformational flexibility can lead to changes in the way the sila-analogue interacts with specific proteins when compared with its parent carbon counterpart, with consequential effects on its pharmacodynamic and pharmacokinetic properties. In the case of lipophilic organic substituents attached to a central carbon atom of a given drug, the corresponding sila-analogue is more lipophilic due to the different covalent radii of carbon and silicon. This change in lipophilicity can modify in many ways the *in vivo* properties of a drug.

Silicon (1.74, Allred–Rochow) is less electronegative than carbon (2.50), leading to different polarizations of analogous carbon–element and silicon–element bonds. These differences can also affect the pharmacodynamics and pharmacokinetics. A special effect is an increase in acidity of a silanol (R<sub>3</sub>Si–OH) compared with that of an analogous alcohol (R<sub>3</sub>C–OH), particularly in those cases where electron-withdrawing substituents are bound to the silicon atom. As a result, the hydrogen bond strength of the silanol will be more favorable as a donor than that of the analogous alcohol. In pharmacophores, in which the COH group functions as a hydrogen bond donor, the carbon/silicon switch (→ SiOH group) can be beneficial in providing improved ligand–receptor binding.

However, there are also some striking differences between carbon and silicon that lead to stability-driven limitations of the carbon/silicon switch strategy. Unlike carbon, silicon can form thermodynamically stable five- or six-coordinate compounds that can be isolated. Conversely, coordination numbers two and three are disfavored over the coordination number four in the case of silicon. Generally,

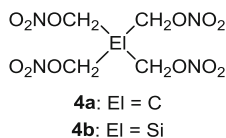


**Fig. 2** Chemical structures of the C/Si analogues **4a** and **4b**

silicon–element double and triple bonds are thermodynamically unstable and can only be kinetically stabilized by very bulky substituents. Thus, replacement of an  $sp$ - or  $sp^2$ -hybridized carbon atom in a drug by a silicon atom is not possible.

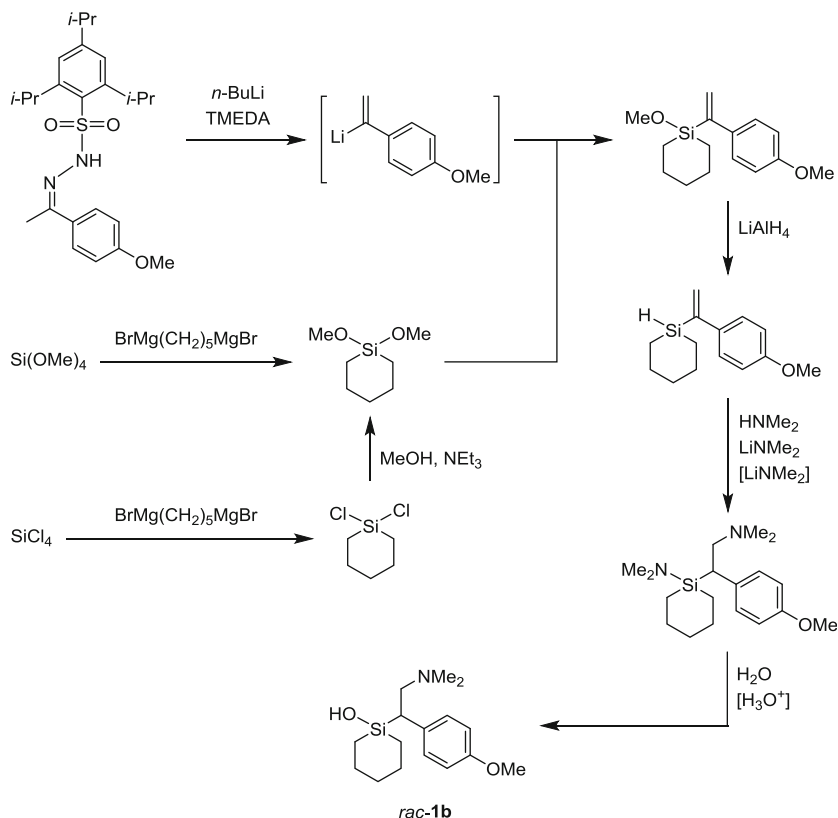
Another limitation concerns the hydrolytic instability of many silicon–element bonds, such as the Si–H, Si–O, Si–S, Si–N, and Si–P bond. Under physiological conditions, these bonds undergo hydrolysis ( $\text{R}_3\text{Si–H} + \text{H}_2\text{O} \rightarrow \text{R}_3\text{Si–OH} + \text{H}_2$ ;  $\text{R}_3\text{Si–XR} + \text{H}_2\text{O} \rightarrow \text{R}_3\text{Si–OH} + \text{HXR}$  ( $\text{X}=\text{O}, \text{S}$ );  $\text{R}_3\text{Si–XR}_2 + \text{H}_2\text{O} \rightarrow \text{R}_3\text{Si–OH} + \text{HXR}_2$  ( $\text{X}=\text{N}, \text{P}$ )). On the other hand, this hydrolytic instability offers possibilities for the development of short-acting drugs that undergo a controlled hydrolytic decomposition. Also, this hydrolytic lability could be useful for prodrug strategies.

In this context, another stability issue (although very special) should be briefly mentioned. Some years ago, the silicon analogue of the coronary vasodilator pentaerythritol tetranitrate (**4a**), sila-pentaerythritol tetranitrate (**4b**), was successfully synthesized but then turned out to be a very dangerous explosive that did not allow any biological characterization (Fig. 2) [23]. The carbon compound **4a** is also shock-sensitive and is a well-known commercial explosive (nitropenta, PENT), but it can be handled relatively easily. In contrast, the silicon analogue **4b** is an extremely shock-sensitive material that is very difficult to handle (for sila-analogues of other explosives, see [24, 25]). This different behavior of the C/Si analogues **4a** and **4b** once again demonstrates that, in spite of the many similarities of carbon and silicon, the carbon/silicon switch can significantly affect the chemical and physicochemical properties.

### 3 Sila-Substitution of Drugs: Selected Examples

#### 3.1 Sila-Venlafaxine: A Silicon Analogue of the Serotonin/ Noradrenaline Reuptake Inhibitor Venlafaxine

Racemic venlafaxine (*rac*-**1a**) is a serotonin/noradrenaline reuptake inhibitor that is in clinical use as an antidepressant. *rac*-Sila-venlafaxine (*rac*-**1b**), a silicon analogue of *rac*-**1a**, was synthesized in multistep syntheses, starting from  $\text{SiCl}_4$  or  $\text{Si}(\text{OMe})_4$  (Scheme 1) [26, 27]. An alternative synthesis of *rac*-**1b**, starting from  $\text{SiCl}_4$ , is shown in Scheme 2 [28, 29]. The single enantiomers of sila-venlafaxine, (*R*)-**1b** and (*S*)-**1b**, were obtained by resolution of *rac*-**1b**, using (+)- and (–)-10-camphorsulfonic acid as resolving agents [26]. The absolute configuration of (*R*)-**1b**

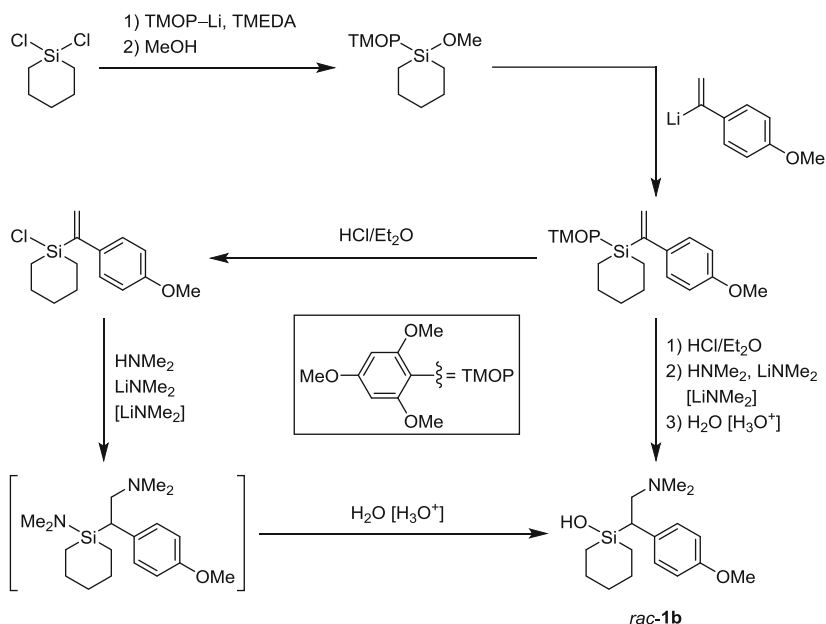


**Scheme 1** Synthesis of *rac-1b*

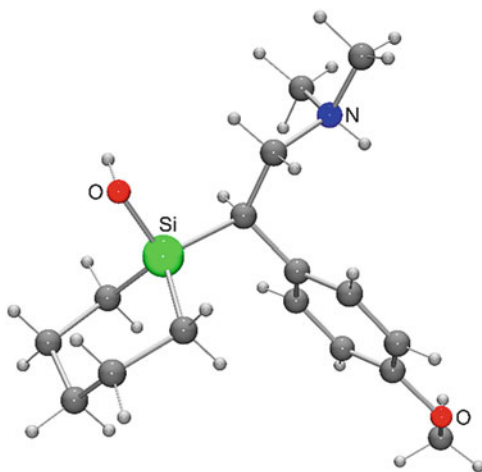
was determined by a crystal structure analysis of the corresponding hydrobromide (*R*)-**1b**·HBr [26]. The molecular structure of the cation of (*R*)-**1b**·HBr is depicted in Fig. 3 [26].

Figure 4 shows a superposition of the cyclohexane skeleton of (*S*)-**1a**·HBr and the 1-silacyclohexane skeleton of the (*S*)-enantiomer of *rac-1b*·HCl (structures determined by single-crystal X-ray diffraction) [26]. Due to the longer covalent radius of the silicon atom, the 1-silacyclohexane ring is more flat than the cyclohexane ring, leading to different relative orientations of the OH and NH groups of the two C/Si analogues. These different structures may affect the ligand–receptor interactions of venlafaxine (**1a**) and sila-venlafaxine (**1b**).

To get information about their physicochemical properties, compounds *rac-1a* and *rac-1b* were studied for their  $\text{pK}_a$ ,  $\log P$ , and  $\log D$  ( $\log P$  at pH 7.4) values [26]. As can be seen from Table 1, very similar physicochemical profiles were observed for the two C/Si analogues, suggesting similar brain penetration profiles of venlafaxine (**1a**) and sila-venlafaxine (**1b**). At pH 7.4 (physiological pH), both compounds exist predominantly in their protonated form (degree of protonation ca. 90%).



**Scheme 2** Synthesis of *rac*-1b



**Fig. 3** Molecular structure of the cation of (*R*)-1b-HBr in the crystal [26]

Compounds (*R*)-1a, (*S*)-1a, (*R*)-1b, and (*S*)-1b were studied for their efficacy in serotonin, noradrenaline, and dopamine reuptake inhibition assays [26]. Human HEK-293 (serotonin), MDCK (noradrenaline), and CHO-K1 (dopamine) cell lines and the radioligands [<sup>3</sup>H]serotonin, [<sup>3</sup>H]noradrenaline, and [<sup>3</sup>H]dopamine,

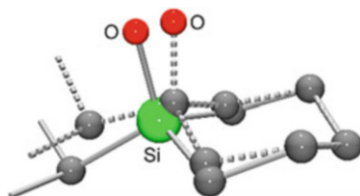


**Fig. 4** Superposition of the cyclohexane skeleton of (*S*)-**1a**·HBr (*dashed bonds*) and the 1-silacyclohexane skeleton of the (*S*)-enantiomer of *rac*-**1b**·HCl (*solid bonds*) (hydrogen atoms are omitted for clarity) [26]

**Table 1**  $pK_a$ ,  $\log P$ , and  $\log D$  ( $\log P$  at pH 7.4) data for *rac*-**1a** and *rac*-**1b** [26]

Compound	$pK_a$	$\log P$	$\log D$
<i>rac</i> - <b>1a</b>	9.7	3.13	0.88
<i>rac</i> - <b>1b</b>	9.7	3.21	0.92

**Table 2** Serotonin, noradrenaline, and dopamine transporter inhibition profiles of (*R*)-**1a**, (*S*)-**1a**, (*R*)-**1b**, and (*S*)-**1b** ( $IC_{50}$ ,  $\mu M$ ) [26]

Compound	Serotonin	Noradrenaline	Dopamine
( <i>R</i> )- <b>1a</b>	0.030	0.061	19.600
( <i>S</i> )- <b>1a</b>	0.006	0.754	6.670
( <i>R</i> )- <b>1b</b>	3.168	0.251	5.270
( <i>S</i> )- <b>1b</b>	0.791	4.715	36.350

The data represent the mean of at least two determinations

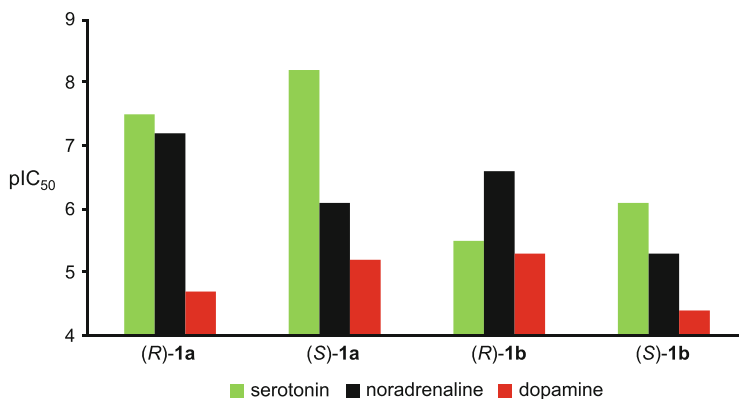


**Fig. 5** In vitro efficacy of (*R*)-**1a**, (*S*)-**1a**, (*R*)-**1b**, and (*S*)-**1b** regarding serotonin, noradrenaline, and dopamine reuptake inhibition [26].  $pIC_{50}$  denotes the negative decadic logarithm of the half-maximum effect concentration (M). The data represent the mean of at least two determinations

respectively, were used in these studies. The results obtained are shown in Table 2 and Fig. 5.

As can be seen from Table 2 and Fig. 5, the sila-venlafaxine enantiomers (*R*)-**1b** and (*S*)-**1b** exhibit a substantially altered monoamine reuptake inhibition profile when compared with the respective venlafaxine enantiomers (*R*)-**1a** and (*S*)-**1a**.

While activity at the noradrenaline and dopamine transporters is only slightly affected by sila-substitution, the potency at the serotonin transporters is reduced by two orders of magnitude, resulting in totally altered selectivity profiles. (*S*)-Venlafaxine ((*S*)-**1a**) is a potent and selective serotonin reuptake inhibitor, being about 100- and 1,000-fold more potent at serotonin transporters than noradrenaline and dopamine transporters, respectively. Sila-substitution of (*S*)-**1a** ( $\rightarrow$  (*S*)-**1b**) makes this compound a rather weak mixed serotonin/noradrenaline reuptake inhibitor, with only about 50- and 6-fold, respectively, selectivity over dopamine and noradrenaline transporters. (*R*)-Venlafaxine ((*R*)-**1a**) is also a mixed serotonin/noradrenaline reuptake inhibitor, with about 500-fold selectivity over dopamine transporters and a significantly higher potency than that of (*S*)-**1b**. Sila-substitution of (*R*)-**1a** ( $\rightarrow$  (*R*)-**1b**) results in a substantially altered selectivity profile. (*R*)-Sila-venlafaxine ((*R*)-**1b**) is a selective noradrenaline reuptake inhibitor being about 10-fold more potent at noradrenaline transporters than at serotonin and dopamine transporters. This is one of the most impressive examples demonstrating that sila-substitution can affect both pharmacological potency and pharmacological selectivity.

To evaluate the potential of the noradrenaline selectivity of (*R*)-sila-venlafaxine ((*R*)-**1b**) for the treatment of various CNS disorders, the compound was profiled further and was tested in vitro across a panel of 68 common receptors/channels and 16 enzymes [30]. In the majority of assays, (*R*)-**1b** was found to be inactive (<50% inhibition at 10  $\mu$ M), including opioid receptors. Only weak affinity at  $\text{Ca}^{2+}$  and  $\text{Na}^{+}$  channels was observed. (*R*)-Sila-venlafaxine ((*R*)-**1b**) was also shown to display only low in vitro activity at the cytochrome P450 enzymes CYP2D6, CYP1A2, CYP2C19, and CYP3A4 (<50 % inhibition at 10  $\mu$ M). In conclusion, (*R*)-**1b** can be indeed regarded as a selective noradrenaline reuptake inhibitor.

Following the idea that this particular selectivity profile may have utility in the treatment of emesis, (*R*)-**1b** was evaluated in a ferret model of morphine-induced emesis [30]. As the C/Si analogues *rac*-**1a** and *rac*-**1b** have almost identical physicochemical properties (Table 1), and based on the evidence that *rac*-**1a** achieves high clinical efficacy in the treatment of depression, one would have high confidence that (*R*)-**1b** would also readily reach its site of action in the CNS. (*R*)-Sila-venlafaxine ((*R*)-**1b**) was dosed orally 2 h prior to the emetogen morphine (0.125 mg/kg, s.c.), and the animals were monitored for retching and vomiting events for up to 2 h following the administration of morphine. At 50 mg/kg, (*R*)-**1b** completely abolished emetic episodes, and almost complete inhibition (93 %) was achieved at 5 mg/kg. In male ferrets, dosed at 5 mg/kg orally, (*R*)-**1b** displayed a plasma half-life of 1.1 h, with a  $C_{\text{max}}$  of 225 ng/ml. In conclusion, the selective noradrenaline reuptake inhibitor (*R*)-sila-venlafaxine ((*R*)-**1b**) has been demonstrated to effectively inhibit emetic episodes caused by an emetogen in a well-characterized in vivo model.

Following this proof of principle, the antiemetic potential of (*R*)-sila-venlafaxine ((*R*)-**1b**) was further evaluated. For this purpose, the potential of (*R*)-**1b** to antagonize cisplatin (15 mg/kg, i.p.)-induced acute and delayed emesis in the ferret was studied [31]. At 5 and 15 mg/kg/4 h (i.p.), (*R*)-**1b** was highly effective in reducing



emetic episodes during the 0–24-h period (acute emesis), and at 15 mg/kg/4 h (i.p.), (*R*)-**1b** was also active to reduce emesis during the 24–72-h period (delayed emesis). These studies provided evidence for an antiemetic potential of the selective noradrenaline reuptake inhibitor (*R*)-sila-venlafaxine ((*R*)-**1b**) to reduce chemotherapy-induced acute and delayed emesis.

### 3.2 Sila-Haloperidol: A Silicon Analogue of the Dopamine Antagonist Haloperidol

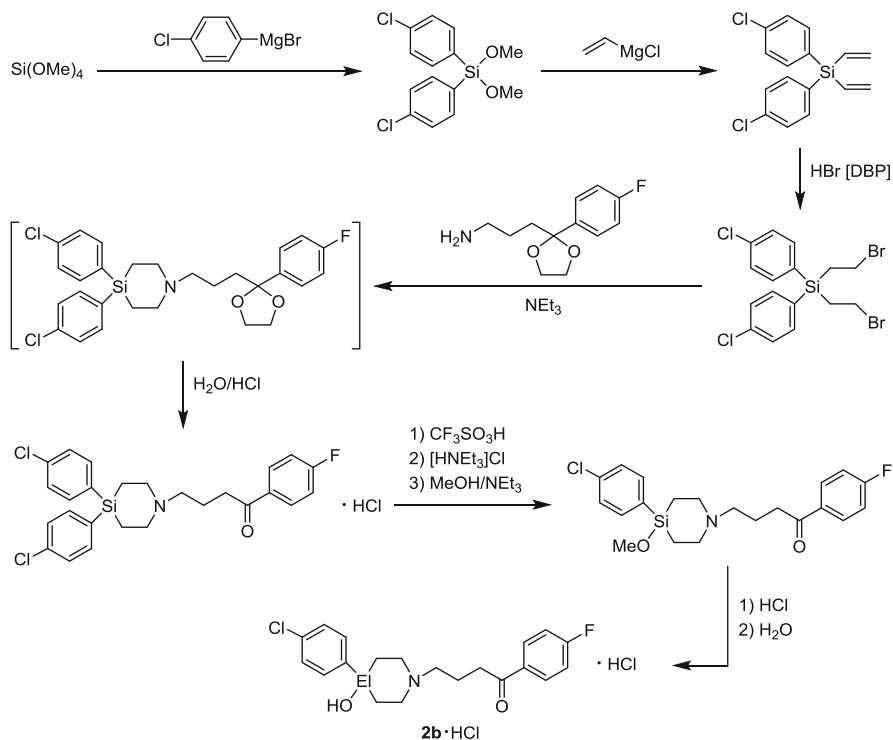
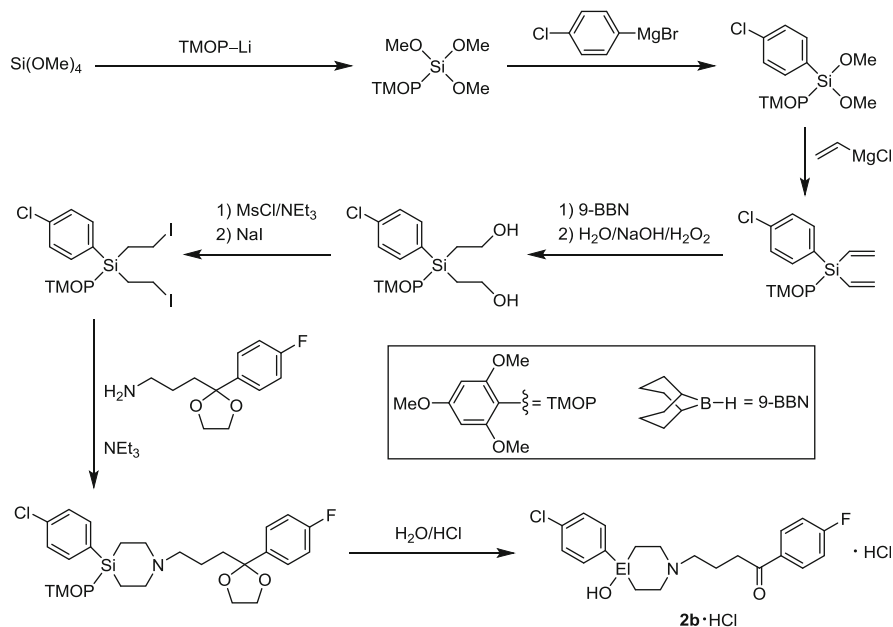
Haloperidol (**2a**) is a dopamine ( $D_2$ ) antagonist that is in clinical use as an antipsychotic agent for the treatment of schizophrenia. Sila-haloperidol (**2b**), a silicon analogue of **2a**, was synthesized in a multistep synthesis, starting from  $\text{Si}(\text{OMe})_4$  (Scheme 3) [32, 33]. An alternative synthesis, also starting from  $\text{Si}(\text{OMe})_4$ , is shown in Scheme 4 [34]. In both cases, sila-haloperidol (**2b**) was isolated as the hydrochloride **2b**·HCl.

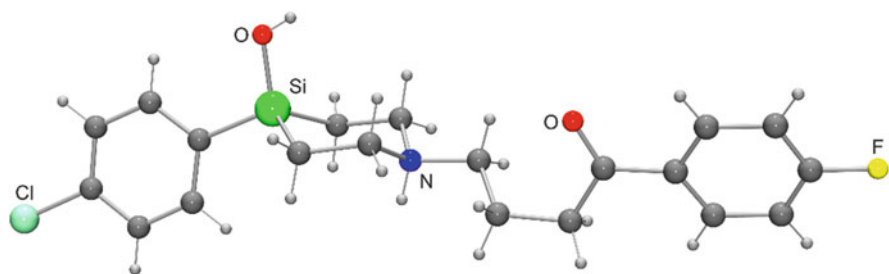
Compound **2b**·HCl was structurally characterized by single-crystal X-ray diffraction [32]. The molecular structure of the cation of **2b**·HCl is depicted in Fig. 6.

Figure 7 shows a superposition of the piperidinium skeleton of **2a**·HCl and the 4-silapiperidinium ring of **2b**·HCl (structures determined by single-crystal X-ray diffraction) [32]. Due to the longer covalent radius of the silicon atom, the 4-silapiperidinium ring is more flat than the piperidinium skeleton, leading to different relative orientations of the *N*-organyl side chain toward the hydroxy and 4-chlorophenyl groups. These different structural features may affect the ligand–receptor interactions of haloperidol (**2a**) and sila-haloperidol (**2b**).

As shown by NMR spectroscopic studies in DMSO at room temperature, two conformers of the piperidinium cation of **2a**·HCl exist in solution (molar ratio ca. 1:13) [32]. This ratio differs significantly from that found for the 4-silapiperidinium cation of **2b**·HCl (molar ratio ca. 1:2), indicating considerable differences in the energies of the respective two conformers of the piperidinium and 4-silapiperidinium ring systems [32]. The structures of the two conformers  $\alpha$  and  $\beta$  are depicted in Fig. 8. The different populations of these two conformers may affect the pharmacological potency of haloperidol (**2a**) and sila-haloperidol (**2b**).

To get information about their physicochemical properties, compounds **2a** and **2b** were studied as hydrochlorides for their  $\text{p}K_a$  and  $\log D$  ( $\log P$  at pH 7.4) values and for their solubility in HBSS buffer (pH 7.4) [34]. As can be seen from Table 3, similar physicochemical profiles were observed for the two C/Si analogues. The apparent permeability ( $P_{\text{app}}$ ) of **2a** and **2b** was also similar (studied in a human Caco-2 model) [34]. In both cases, the  $P_{\text{app}}$  values were high (**2a**,  $P_{\text{app}} = 18.9 \times 10^{-6} \text{ cm s}^{-1}$ ; **2b**,  $P_{\text{app}} = 19.8 \times 10^{-6} \text{ cm s}^{-1}$ ), and the recovery rate was around 90%, indicating that both compounds passed the cellular barrier more or less unchanged. As haloperidol (**2a**) is known to possess good bioavailability in humans, these results suggest a high permeability for sila-haloperidol (**2b**) as well.

Scheme 3 Synthesis of **2b**·HClScheme 4 Synthesis of **2b**·HCl



**Fig. 6** Molecular structure of the cation of **2b**-HCl in the crystal [32]

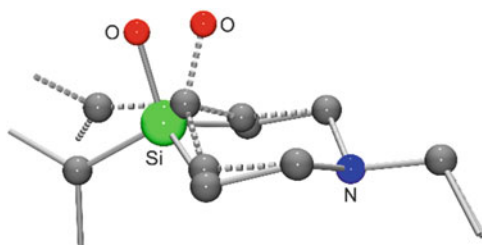


**Fig. 7** Superposition of the piperidinium skeleton of **2a**-HCl (*dashed bonds*) and the 4-silapiperidinium skeleton of **2b**-HCl (*solid bonds*) (hydrogen atoms are omitted for clarity) [32]

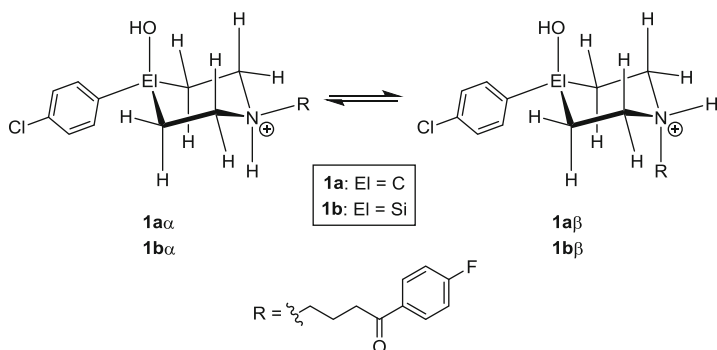


**Fig. 8** Conformers  $\alpha$  and  $\beta$  of the piperidinium skeleton of **2a**-HCl and the 4-silapiperidinium skeleton of **2b**-HCl [32]

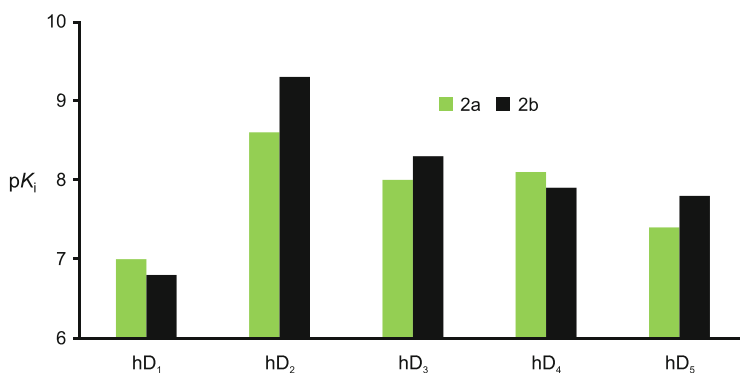
Haloperidol (**2a**) and sila-haloperidol (**2b**) were studied for their affinities at all five human dopamine receptors in competitive radioligand receptor binding assays [34]. The results obtained are shown in Table 4 and Fig. 9. All Hill slopes were not significantly different from unity, thus assuming a single binding site for **2a** and **2b** at all receptors.

**Table 3**  $pK_a$ ,  $\log D$  ( $\log P$  at pH 7.4), and solubility (in HBSS buffer at pH 7.4) data for **2a** and **2b** [34]

Compound	$pK_a$	$\log D$	Solubility ( $\mu M$ )
<b>2a</b>	$9.07 \pm 0.07$	$2.42 \pm 0.03$	$90 \pm 2$
<b>2b</b>	$9.27 \pm 0.10$	$2.77 \pm 0.13$	$78 \pm 7$

**Table 4** Affinities of **2a** and **2b** at human dopamine receptors [34]

Receptor subtype	$K_i$ (nM) for <b>2a</b>	$K_i$ (nM) for <b>2b</b>
hD <sub>1</sub>	$107 \pm 22.0$	$162 \pm 34.5$
hD <sub>2</sub>	$2.84 \pm 0.26$	$0.55 \pm 0.06$
hD <sub>3</sub>	$10.4 \pm 1.47$	$4.73 \pm 0.51$
hD <sub>4</sub>	$7.94 \pm 0.69$	$14.1 \pm 1.09$
hD <sub>5</sub>	$38.0 \pm 4.72$	$16.6 \pm 3.20$

**Fig. 9** Affinities of **2a** and **2b** at human dopamine receptors [34]

As can be seen from Table 4 and Fig. 9, sila-haloperidol (**2b**) shows a significantly higher affinity for hD<sub>2</sub> receptors than haloperidol (5.1-fold), whereas the silicon compound **2b** is approximately equipotent to its carbon analogue **2a** at all the other dopamine receptors (differences are less than 2.3-fold). As a result, the subtype selectivity of **2b** for hD<sub>2</sub> over the other dopamine receptors is somewhat higher than that of **2a** (Fig. 10). Sila-haloperidol (**2b**) has an approximately 2-fold higher selectivity than haloperidol (**2a**) for D<sub>2</sub> over D<sub>3</sub> and D<sub>2</sub> over D<sub>5</sub> but an 8- to 9-fold higher selectivity for D<sub>2</sub> over D<sub>1</sub> and D<sub>2</sub> over D<sub>4</sub> relative to **2a**.

The C/Si analogues **2a** and **2b** were also characterized by functional studies at human dopamine D<sub>1</sub> and D<sub>2</sub> receptors using a calcium fluorimetric functional assay [35]. The functional data for **2a** (hD<sub>1</sub>,  $K_i = 398$  nM; hD<sub>2</sub>,  $K_i = 0.36$  nM) and **2b** (hD<sub>1</sub>,  $K_i = 194$  nM; hD<sub>2</sub>,  $K_i = 0.12$  nM) were similar to the binding data (Table 4). None of the compounds displayed any agonist activity at D<sub>1</sub> or D<sub>2</sub> receptors.

To further characterize the pharmacodynamic properties of **2a** and **2b**, the two C/Si analogues were also studied for their  $\sigma_1$  (guinea pig brain) and  $\sigma_2$  (rat liver) receptor affinities using competitive radioligand receptor binding assays (Table 5)

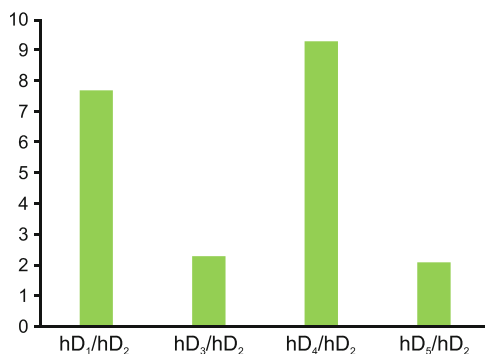


**Fig. 10** Ratios of the subtype selectivities hD<sub>1</sub>/hD<sub>2</sub>, hD<sub>3</sub>/hD<sub>2</sub>, hD<sub>4</sub>/hD<sub>2</sub>, and hD<sub>5</sub>/hD<sub>2</sub> of **2a** and **2b**, shown as **2a/2b** ratios [34]

**Table 5** Affinities of **2a** and **2b** at  $\sigma_1$  (guinea pig brain) and  $\sigma_2$  receptors (rat liver) [34]

Receptor subtype	$K_i$ (nM) for <b>2a</b>	$K_i$ (nM) for <b>2b</b>
$\sigma_1$	$1.9 \pm 0.4$	$3.4 \pm 0.4$
$\sigma_2$	$78.1 \pm 2.4$	$309 \pm 55$

[34]. At the  $\sigma_1$  receptor, **2a** and **2b** are approximately equipotent, whereas **2a** exhibits a 4-fold higher affinity for the  $\sigma_2$  receptor than the silicon analogue **2b**. As a result, the subtype selectivity of sila-haloperidol (**2b**) for the  $\sigma_1$  over the  $\sigma_2$  receptor is approximately 3-fold higher than that of haloperidol (**2a**).

In conclusion, in comparison with haloperidol (**2a**), sila-haloperidol (**2b**) shows a higher potency at dopamine D<sub>2</sub> receptors and a higher subtype selectivity at both dopamine and  $\sigma$  receptors.

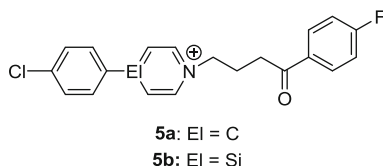
To determine the rate of decomposition of haloperidol (**2a**) and sila-haloperidol (**2b**) in vitro, the intrinsic clearance and half-lives were measured in human and female rat liver microsomes [34]. As can be seen from Table 6, the C/Si analogues **2a** and **2b** showed a similar moderate stability in the presence of human liver microsomes. However, decomposition in the presence of rat liver microsomes was significantly increased by sila-substitution.

Haloperidol (**2a**) and sila-haloperidol (**2b**) were also studied for their CYP inhibition of the five major isoforms of cytochrome P450 [34]. No CYP inhibition of either **2a** or **2b** against CYP1A2, CYP2C9, and CYP2C19 could be detected ( $IC_{50} > 20 \mu M$ ). However, the silicon compound **2b** showed an almost 3-fold increased inhibitory potency against CYP3A4 ( $IC_{50} = 9.6 \pm 1.4 \mu M$ ) compared to the carbon analogue **2a** ( $IC_{50} = 26.2 \pm 7.9 \mu M$ ). CYP2D6 was also inhibited by **2a** and **2b**, with almost identical  $IC_{50}$  values (**2a**,  $2.1 \pm 0.6 \mu M$ ; **2b**,  $1.7 \pm 0.9 \mu M$ ).

Haloperidol (**2a**) and sila-haloperidol (**2b**) were also investigated for their in vitro metabolism [34, 36]. It is known that one of the major metabolites of **1a**, the pyridinium species HPP<sup>+</sup> (**5a**, Fig. 11), has neurotoxic properties and is suspected to cause severe extrapyramidal side effects, including Parkinsonism and tardive dyskinesia. As a matter of principle, an analogous metabolite of the

**Table 6** Intrinsic clearance  $Cl_{\text{int}}$  ( $\mu\text{L min}^{-1} \text{mg}^{-1}$ ) and half-life  $t_{1/2}$  (min) of **2a** and **2b** in human and rat liver microsomes [34]

Compound	$Cl_{\text{int hu}}$	$Cl_{\text{int rat}}$	$t_{1/2 \text{ hu}}$	$t_{1/2 \text{ rat}}$
<b>2a</b>	$20 \pm 2$	$21 \pm 5$	51	65
<b>2b</b>	$21 \pm 2$	$78 \pm 7$	65	18

**Fig. 11** Chemical structures of the C/Si analogues **5a** and **5b**

silicon analogue **2b**, the silapyridinium species sila-HPP<sup>+</sup> (**5b**, Fig. 11), cannot be formed, because the silicon–carbon double bond is unstable [32].

The phase I metabolism of haloperidol (**2a**) and sila-haloperidol (**2b**) was investigated in rat and human liver microsomes [34, 36]. The phase II metabolism of **2a** and **2b** was studied in rat, dog, and human hepatocytes and also in rat and human liver microsomes supplemented with UDP-glucuronic acid (UDPGA) [36]. These studies were performed using mass-spectrometric techniques. The structures of the proposed metabolites were assigned based on accurate mass measurements and interpretation of MS–MS spectra. The relative metabolite amounts were estimated by integration of extracted ion chromatograms and refer to the respective fractions metabolized.

The phase I and II metabolism of sila-haloperidol (**2b**) differs significantly from that of haloperidol (**2a**). This is demonstrated exemplarily in Figs. 12 and 13, where the major metabolites in human liver microsomes (incubation time 60 min) and human hepatocytes (incubation time 120 min) are shown.

For the carbon compound **2a**, the pyridinium metabolite **5a** was identified as a major metabolite in the microsomal incubations. The analogous silapyridinium metabolite **5b** was not formed. Instead, two ring-opened metabolites, the silanediols **6** and **7**, were observed. These two metabolites were the major metabolites of sila-haloperidol (**2b**) in human liver microsomes, followed by the *N*-dealkylated metabolite **8b**. The corresponding carbon analogue **8a** was also observed in microsomal incubations of haloperidol (**2a**).

Figure 14 shows the proposed pathway for the metabolic ring opening of sila-haloperidol (**2b**) to give the silanediols **6** and **7** [36]. By analogy to the pathway leading to the pyridinium metabolite of haloperidol (**2a**), the metabolism of the silapiperidine ring of the silicon analogue **2b** is most likely initiated by an enzymatic hydroxylation at the  $\beta$ -carbon atom ( $\beta$  to the silicon atom), followed by ring opening (C–N bond cleavage) to form an intermediate with an aldehyde and a secondary amine functionality. This intermediate, an  $\alpha$ -silylaldehyde, is very reactive and easily undergoes hydrolytic cleavage of the Si–C bond. The proposed

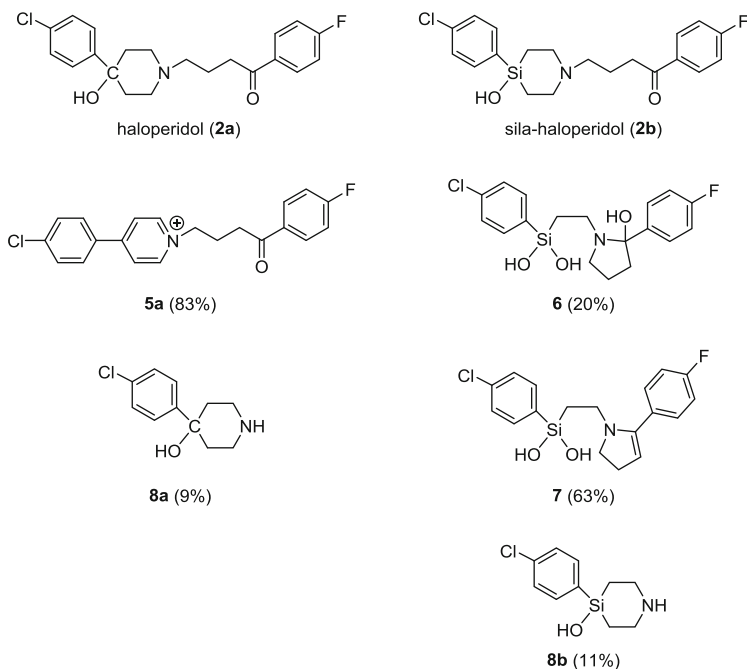


**Fig. 12** Major metabolites of the C/Si analogues **2a** and **2b** in human liver microsomes. Relative metabolite amounts of the respective fraction metabolized (**2a**, 41%; **2b**, 35%) are given in percent [36]

cyclization following the elimination of acetaldehyde then yields the metabolite **6**, which upon water elimination affords **7**.

The major metabolites of haloperidol (**2a**) in hepatocytes were the pyridinium metabolite **5a**, the *N*-dealkylated metabolite **8a**, reduced haloperidol (**2a**) (metabolite **9a**), and the glucuronidation metabolite **10** (not observed in dog hepatocytes). Reduced sila-haloperidol (**2b**) (metabolite **9b**) was the major metabolite in the dog and human hepatocytes, whereas the *N*-dealkylated metabolite **8b** and a metabolite originating from hydroxylation and glucuronidation were the major metabolites in rat hepatocytes. The metabolites **8b** and **9b** were found in all hepatocytes, and the ring-opened metabolites **6** and **7** were only formed in dog and human hepatocytes.

While haloperidol (**2a**) undergoes a direct glucuronidation of the OH group in rat and human hepatocytes and in rat and human liver microsomes supplemented with UDPGA, an analogous glucuronide conjugation was not observed for sila-haloperidol (**2b**). One could speculate that the direct glucuronidation of the SiOH group of **2b** occurs but that the resulting conjugate with its hydrolytically sensitive Si–OC bond then undergoes a spontaneous hydrolysis to give **2b** and free glucuronic acid. In this context, it is important to note that the chemical reactivity of the thermodynamically very stable (but against water kinetically labile) Si–OC bond of alkoxysilanes (alkyl silyl ethers) differs significantly from that of the C–OC bond of analogous dialkyl ethers. An alternative explanation for the absence of

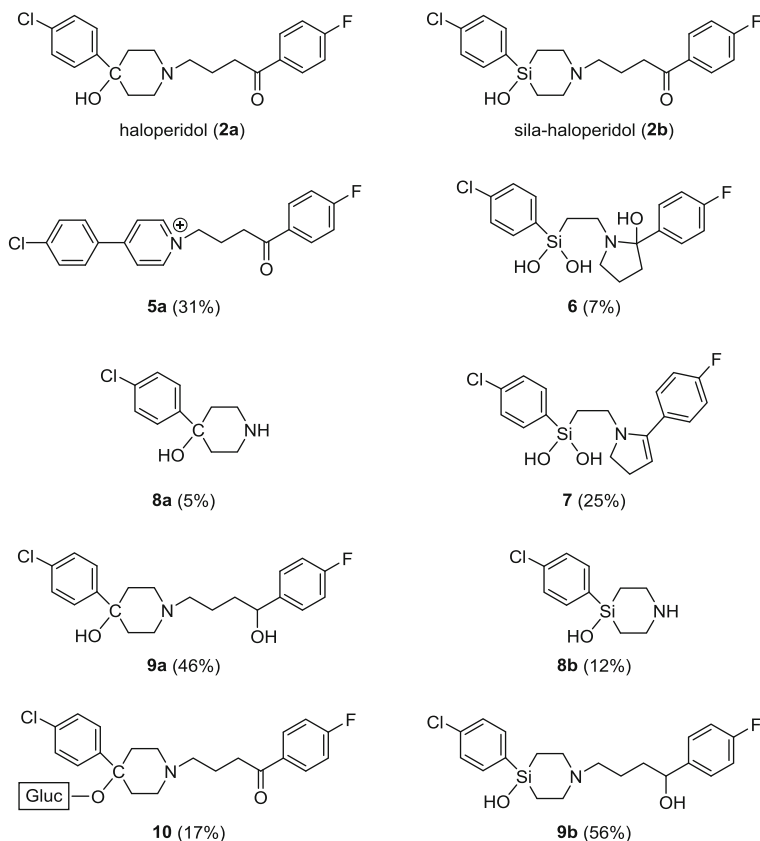


**Fig. 13** Major metabolites of the C/Si analogues **2a** and **2b** in human hepatocytes. Relative metabolite amounts of the respective fraction metabolized (**2a**, 14%; **2b**, 6%) are given in percent [36]

glucuronidation of the SiOH group of sila-haloperidol (**2b**) might be that **2b** is a poor substrate for the UDP-glucuronosyltransferases. Anyway, these results clearly demonstrate that sila-substitution of haloperidol (**2a**) strongly affects the phase II metabolism.

In conclusion, haloperidol (**2a**) and sila-haloperidol (**2b**) differ significantly in their phase I and II metabolism. These differences can be directly correlated with the silicon-specific reactivity profile of **2b**. Studies on the in vitro metabolism of the structurally related dopamine (D<sub>2</sub>) antagonists trifluoperidol (**11a**) and sila-trifluoperidol (**11b**) led to similar results (Fig. 15) [36].



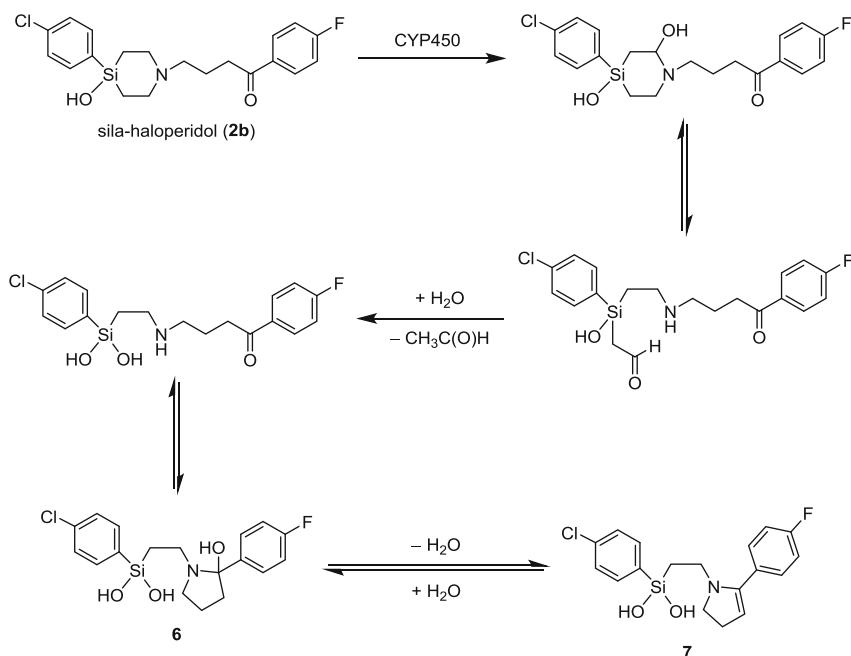


**Fig. 14** Proposed mechanism for the metabolic ring opening of sila-haloperidol (**2b**) to give the silanediol metabolites **6** and **7** [36]

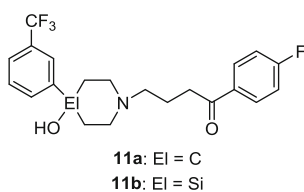
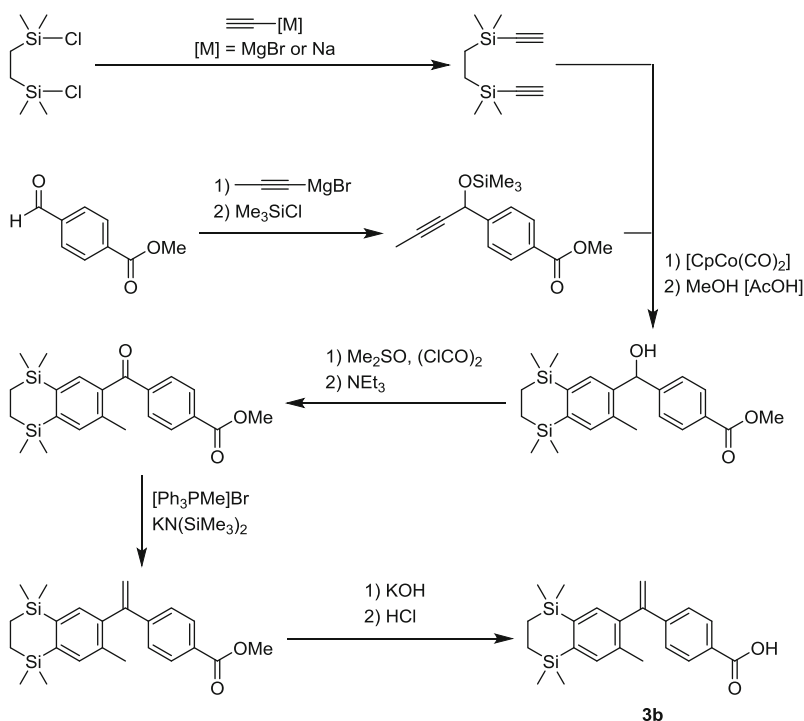


**Fig. 15** Chemical structures of the C/Si analogues **11a** and **11b**

### 3.3 Disila-Bexarotene: A Silicon Analogue of the Retinoid Agonist Bexarotene

Bexarotene (**3a**) is an RXR-selective retinoid agonist that is in clinical use for the treatment of cutaneous T-cell lymphoma. Disila-bexarotene (**3b**), a silicon analogue of **3a**, was synthesized in a multistep synthesis, starting from  $\text{ClMe}_2\text{Si}(\text{CH}_2)_2\text{SiMe}_2\text{Cl}$  (Scheme 5) [37, 38]. An alternative synthesis, also starting from  $\text{ClMe}_2\text{Si}(\text{CH}_2)_2\text{SiMe}_2\text{Cl}$ , is shown in Scheme 6 [39].

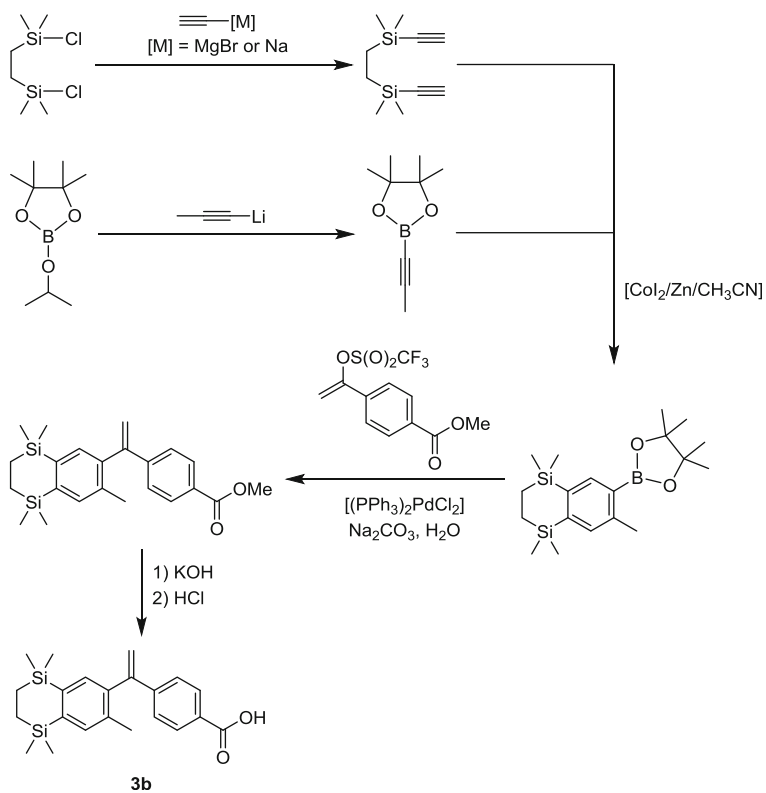
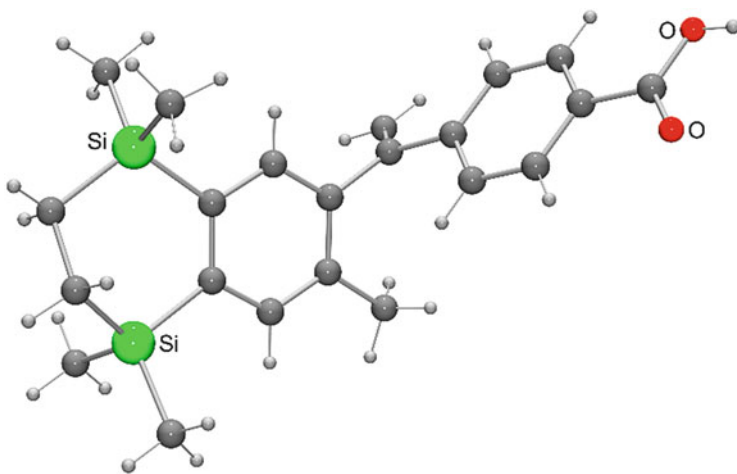
Compound **3b** was structurally characterized by single-crystal X-ray diffraction [37]. The molecular structure of **3b** is depicted in Fig. 16.



**Scheme 5** Synthesis of **3b**

Figure 17 shows a superposition of the tetrahydronaphthalene skeleton of **3a** and the tetrahydrodisilanaphthalene skeleton of **3b** (structures determined by single-crystal X-ray diffraction) [37]. Due to the longer covalent radius of the silicon atom, the two molecular frameworks differ in their size and shape. As shown by experimental [40] and computational [41] studies, disila-substitution of bexarotene (**3a**) also affects the electronic structure (electrostatic potential) of the bicyclic skeleton. As the tetrahydronaphthalene ring of **3a** and structurally related retinoid agonists is known to play a crucial role in receptor binding, the structural and electronic differences between bexarotene (**3a**) and disila-bexarotene (**3b**) may affect the ligand–receptor interactions of these two C/Si analogues.

As a proof of principle, compounds **3a** and **3b** were studied for their RXR $\beta$  agonistic potency in a HeLa cell-based receptor assay [37]. The cell line was engineered to express a chimeric receptor composed of the DNA binding domain of the GALA4 yeast transcription factor and the ligand binding domain of human RXR $\beta$  (GALA4-hRXR $\beta$ ). In these studies, the natural ligand 9-*cis*-retinoic acid (9-*cis*RA) served as the positive control. As can be seen from Fig. 18, bexarotene (**3a**) is more potent than 9-*cis*-retinoic acid, and disila-bexarotene (**3b**) has a profile comparable to that of its carbon analogue **3a**. Thus, despite of the structural and electronic changes upon C/Si exchange, very similar RXR $\beta$  agonistic potencies of the C/Si analogues **3a** and **3b** were observed.

**Scheme 6** Synthesis of **3b****Fig. 16** Molecular structure of **3b** in the crystal [37]

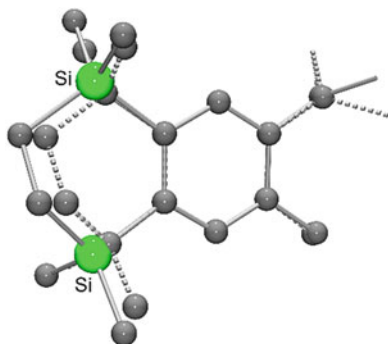


**Fig. 17** Superposition of the tetrahydronaphthalene skeleton of **3a** (*dashed bonds*) and the tetrahydrodisilanaphthalene skeleton of **3b** (*solid bonds*) (hydrogen atoms are omitted for clarity) [37]

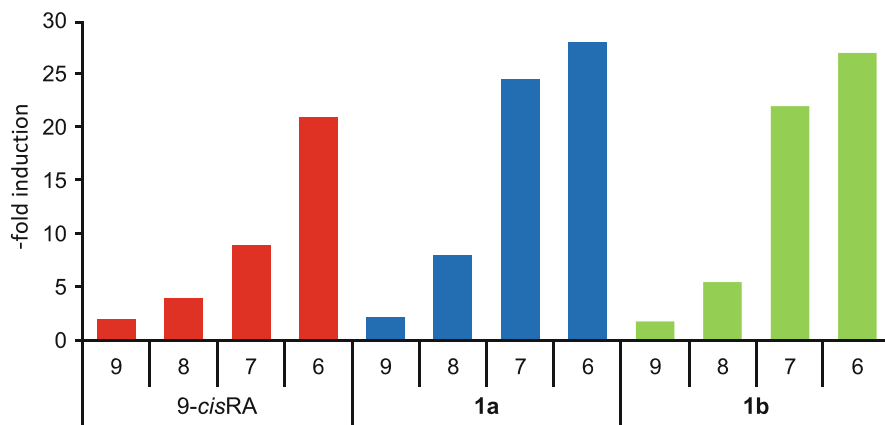


**Fig. 18** Concentration-dependent RXR $\beta$  agonistic potency of 9-*cis*-retinoic acid (9-*cis*RA), bexarotene (**3a**), and disila-bexarotene (**3b**). The data were obtained using a HeLa cell-based receptor assay [37]

As shown in a more recent study, bexarotene (**3a**) may partially act to induce cell differentiation and cell death pathways in pluripotent TERA2.cl.SP12 stem cells [42]. However, disila-bexarotene (**3b**) did not show the ability to induce stem cell differentiation in this study but may possess some enhanced functions over **3a**, such as cell death induction and regulation of cell numbers [42].

As disila-substitution of bexarotene (**3a**  $\rightarrow$  **3b**) did not lead to any detrimental effects on the biological activity in terms of its ability to activate target genes through the RXR receptor [37], these studies were extended, and a series of further disila-analogues of retinoid agonists (both RXR and RAR agonists) was synthesized and studied for their biological activity: disila-TTNPB (**12b**) [43], disila-3-methyl-TTNPB (**13b**) [43], disila-SR11237 (**14b**) [41], disila-tamibarotene (disila-AM80, **15b**) [44], disila-AM580 (**16b**) [44], disila-EC23 (**17b**) [45], and disila-TTNN (**18b**)

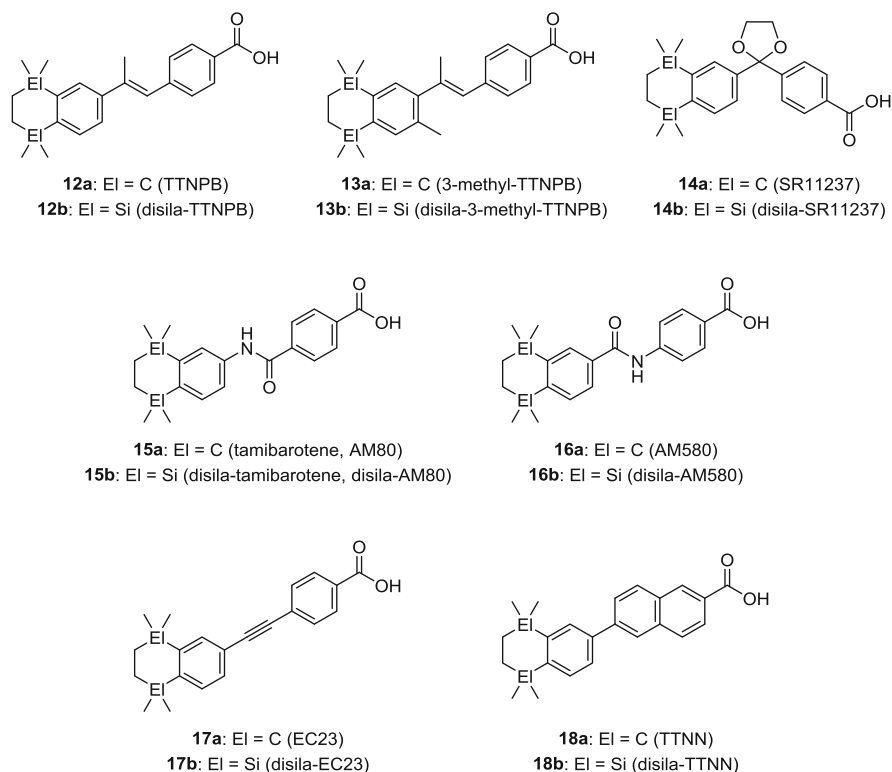


**Fig. 19** Chemical structures of the C/Si pairs **12a/12b–18a/18b**

[45] – the silicon analogues of the retinoid agonists TTNPB (**12a**), 3-methyl-TTNPB (**13a**), SR11237 (**14a**), tamibarotene (AM80, **15a**), AM580 (**16a**), EC23 (**17a**), and TTNN (**18a**), respectively (Fig. 19).

In these studies, some of the tested silicon compounds showed an enhanced agonistic potency compared to the parent carbon compounds. For example, as can be seen from Fig. 20, 2-fold sila-substitution of the pan-RXR-selective retinoid agonist SR11237 (**14a** → **14b**) resulted in an increased RXR $\beta$  agonistic potency [41]. Whereas the dose–response curves of the C/Si analogues **14a** and **14b** are very similar up to 10 nM, there is a stronger activation by the silicon compound **14b** at higher concentrations. This difference in the activities is even more pronounced for the related C/Si analogues **19a** and **19b** (Fig. 21) [41]. As shown in Fig. 20, 2-fold sila-substitution of **19a** (→ **19b**) resulted in a 10-fold increased RXR $\beta$  agonistic potency. It is worth noting that at low concentrations **19b** is even more potent than the natural ligand 9-*cis*RA, which served as the positive control. The 10-fold higher activity of the silicon compound **19b** could be explained with an increased receptor affinity of **19b**, which is in line with the results of crystal structure analyses of the ternary complexes formed by **19a** and **19b**, respectively, with the ligand binding domain of hRXR $\alpha$  and a peptide of the co-activator TIF2/GRIP1 [41]. These

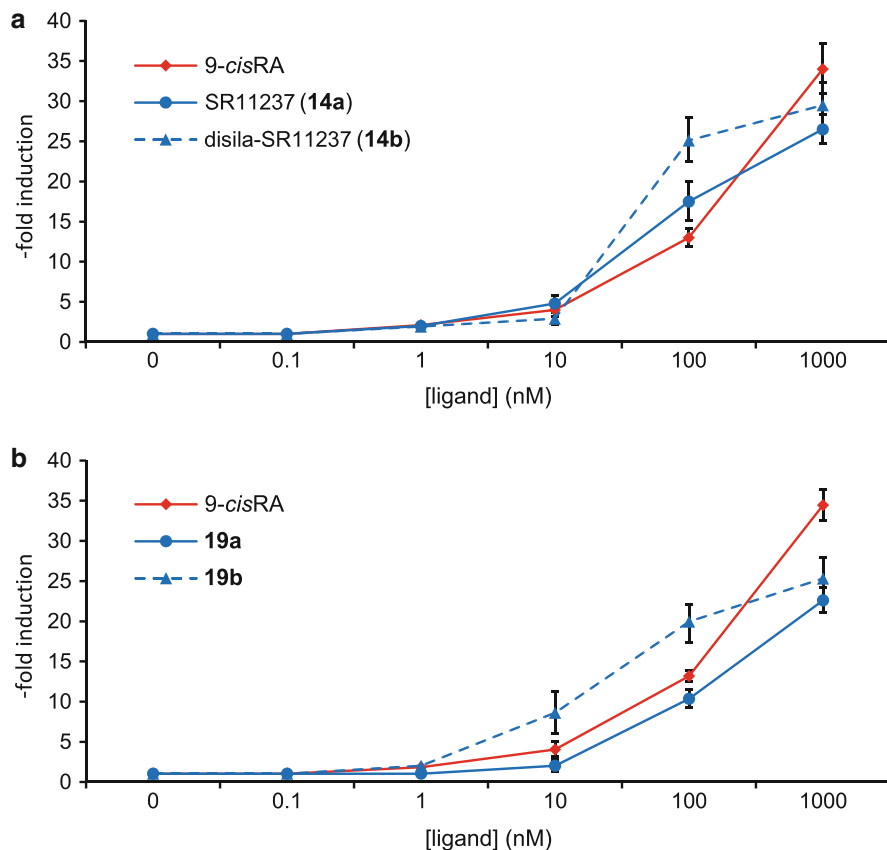


**Fig. 20** Dose–response curves for the transcription activation of RXR $\beta$  by (a) SR11237 (**14a**) and disila-SR11237 (**14b**) and by (b) **19a** and **19b** [38]. 9-*cis*-Retinoic acid (9-*cis*RA) served as the positive control. For the HeLa cell-based receptor assay, see [37]

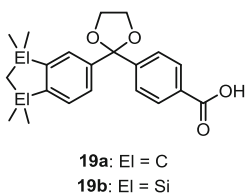


**Fig. 21** Chemical structures of the C/Si analogues **19a** and **19b**

structural investigations revealed additional interactions of **19b** with the H7 and H11 residues. In contrast, crystal structure analyses of the ternary complexes formed by TTNPB (**12a**) and disila-TTNPB (**12b**), respectively, with the ligand binding domain of hRAR $\beta$  and a peptide of the co-activator SRC-1 revealed nearly

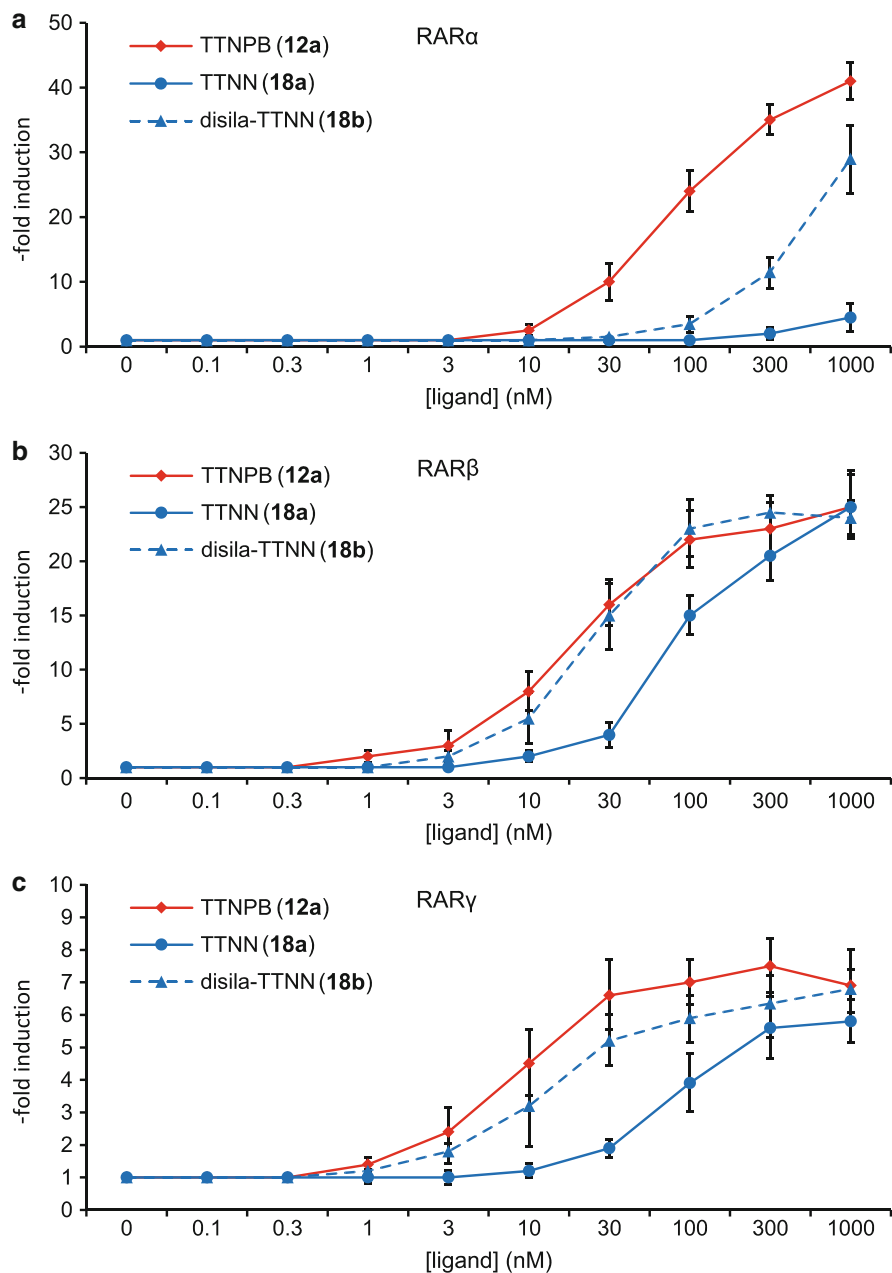


**Fig. 22** Dose-response curves for the transcription activation of (a) hRAR $\alpha$ , (b) hRAR $\beta$ , and (c) hRAR $\gamma$  by TTNN (18a) and disila-TTNN (18b) [45]. TTNPB (12a) served as the positive control

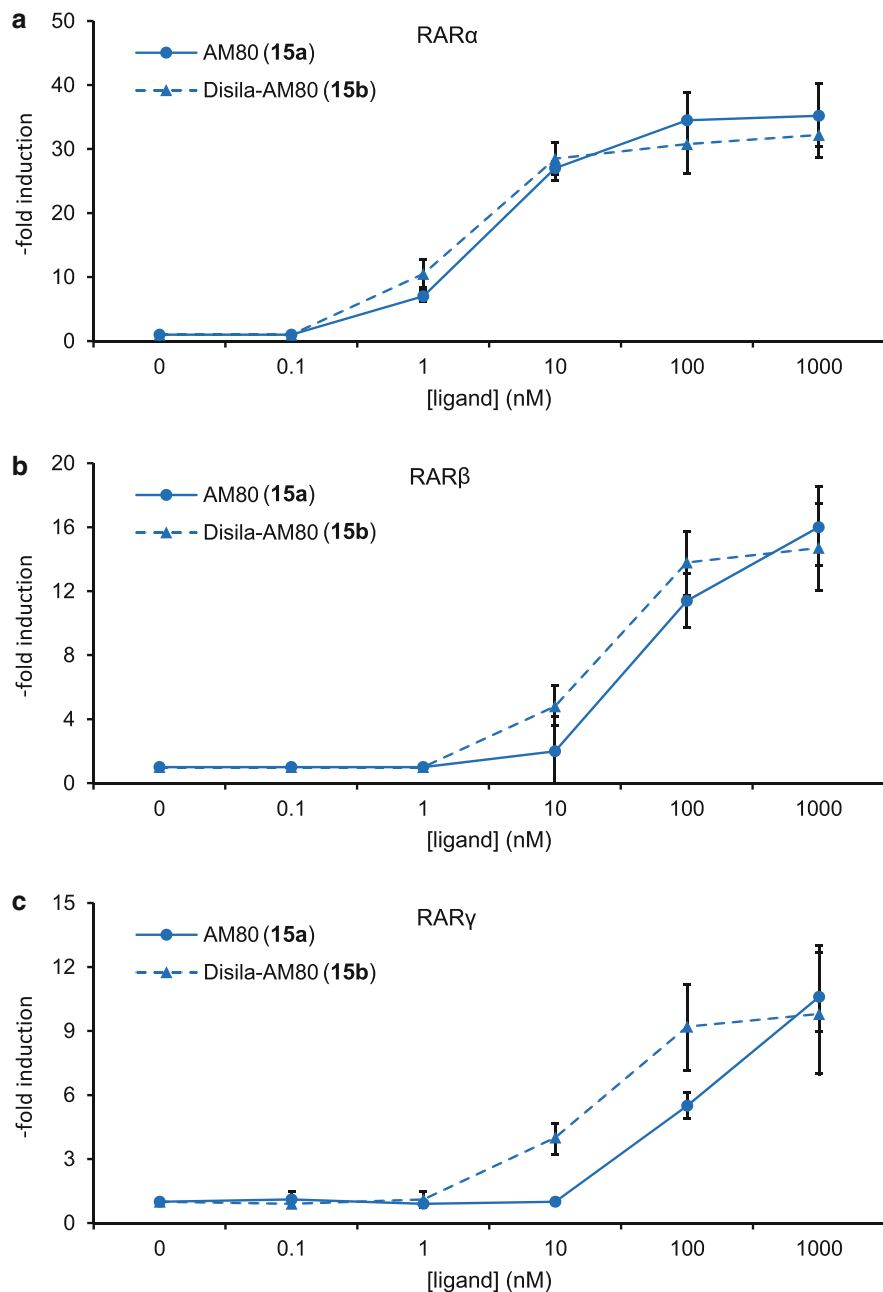


**Fig. 23** Dose–response curves for the transcription activation of (a) hRAR $\alpha$ , (b) hRAR $\beta$ , and (c) hRAR $\gamma$  by tamibarotene (AM80, **15a**) and disila-tamibarotene (disila-AM80, **15b**) [44]



isomorphous structures [43]. This finding correlates with the very similar agonistic potencies of the C/Si analogues **12a** and **12b** at RAR $\alpha$ , RAR $\beta$ , and RAR $\gamma$ , respectively. Compounds **12a** and **12b** were also studied as differentiation- and apoptosis-inducing agents on the basis of their RAR $\alpha$  receptor-activation potential [43]. Upon exposure of NB4 acute promyelocytic leukemia cells to TTNPB (**12a**) and disila-TTNPB (**12b**), respectively, the same strong induction of differentiation and apoptosis of these cells was observed for **12a** and **12b**, which is again in line with the results of the abovementioned structural investigations.

As can be seen from Fig. 22, disila-substitution of the weak retinoid agonist TTNN (**18a**  $\rightarrow$  **18b**) resulted in a significant gain in transcription activation potential for hRAR $\alpha$ , hRAR $\beta$ , and hRAR $\gamma$  [45]. Disila-TTNN (**18b**) can be regarded as a powerful RAR $\beta$ , $\gamma$ -selective retinoid agonist, displaying a similar potency as the powerful reference compound TTNPB (**12a**), which served as the positive control.

In the case of the RAR $\alpha$ -selective retinoid agonist tamibarotene (AM80, **15a**), disila-substitution ( $\rightarrow$  **15b**) did affect not only the agonistic potency but also the retinoid receptor selectivity [44]. Figure 23 shows the dose–response curves of **15a** and **15b** in RAR $\alpha$ , RAR $\beta$ , and RAR $\gamma$  reporter cells. In the case of RAR $\alpha$ , both compounds inhibited virtually identical profiles, with EC<sub>50</sub> values around 5 nM. However, in the case of RAR $\beta$  and even more pronounced for RAR $\gamma$ , there was a significant left shift of the dose–response curves of the silicon compound **15b**. In the case of RAR $\gamma$ , disila-tamibarotene (disila-AM80, **15b**) displayed an up to 10-fold higher activity. As a result, the RAR $\alpha$  selectivity of tamibarotene (AM80, **15a**) is reduced upon disila-substitution. Similar results were also observed for the C/Si analogues AM580 (**16a**) and disila-Am580 (**16b**) [44].

### 3.4 Structures of Other Sila-Drugs

To demonstrate the structural diversity of other sila-analogues of drugs that have been synthesized and biologically characterized in recent years, a series of selected C/Si pairs is compiled in Fig. 24: the muscarinic antagonists **20a/20b** [46], **21a/21b** [46], and **22a/22b** [47]; the  $\sigma$  receptor ligands **23a/23b–26a/26b** [48]; the calcium channel antagonists niguldipine (**27a**) and sila-niguldipine (**27b**) [49]; the histaminic H<sub>1</sub> antagonists terfenadine (**28a**), sila-terfenadine-A (**28b**), sila-terfenadine-B (**28c**), disila-terfenadine (**28d**), fexofenadine (**29a**), and sila-fexofenadine (**29b**) [50]; the  $\sigma$  receptor ligands panamesine (**30a**) and sila-panamesine (**30b**) [51]; the GnRH antagonists AG-045572 (**31a**) and disila-AG-045572 (**31b**) [52]; the antiviral agents **32a/32b–35a/35b** [53]; the antiallergic agents **36a/36b** [54]; the  $\sigma$  receptor ligands **37a/37b–40a/40b** [55]; the estrogenic agents **41a/41b** [56]; and the androgen receptor antagonists LG190178 (**42a**), sila-LG190178 (**42b**), LG190176 (**43a**), and sila-LG190176 (**43b**) [57].

The collection of these compounds shall emphasize the high synthetic potential of modern organosilicon chemistry. This field is rapidly developing, and a huge variety of new classes of organosilicon compounds have been synthesized in recent

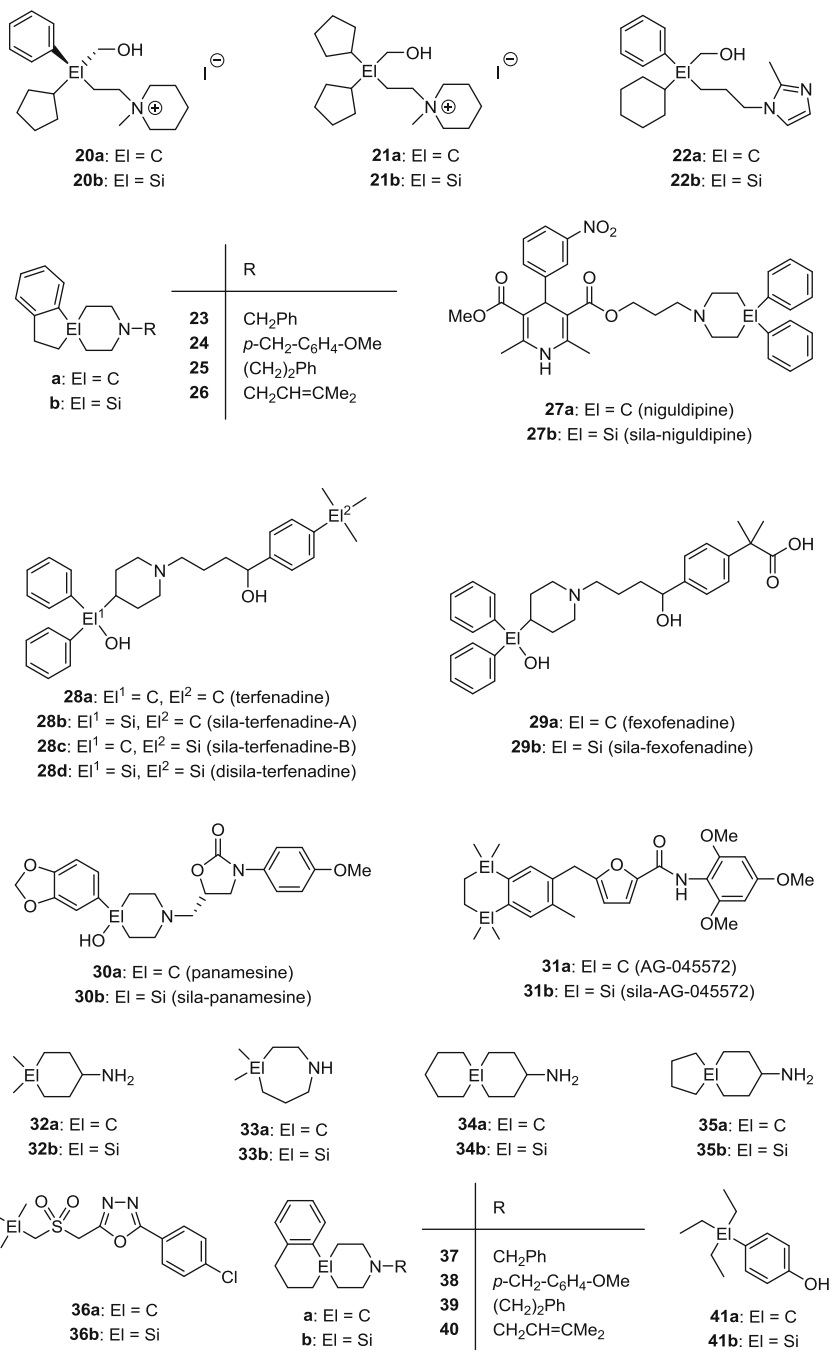
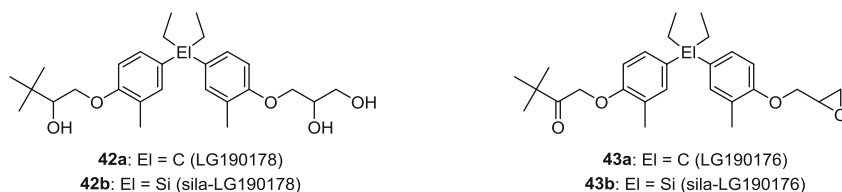


Fig. 24 (continued)



**Fig. 24** Chemical structures of the C/Si pairs **20a/20b–43a/43b**, **28a/28c**, and **28a/28d**

years, and many novel silicon-based molecular scaffolds for drug design will be seen in the near future. In this context, it should also be mentioned that there is an efficient chemical industry, with a special expertise in organosilicon chemistry, that supports this development and can supply pharmaceutical industry with the silicon-based fine chemicals needed.

## 4 Appendix: Sila-Substitution of Odorants

In context with the studies reported in this article, it should be mentioned that the carbon/silicon switch strategy has also successfully been used for the design of silicon-based odorants. As odorant recognition is also based on ligand–receptor interactions (in this case between odorants and olfactory receptors), this approach follows similar principles as described for the design of sila-drugs. To demonstrate the structural diversity of sila-analogues of odorants that have been synthesized and olfactorily characterized in recent years, a series of selected C/Si pairs is compiled in Fig. 25: the musk odorants versalide (**44a**) and disila-versalide (**44b**) [58]; the lily-of-the-valley odorants bourgeonal (**45a**), sila-bourgeonal (**45b**), lilial (**46a**), and sila-lilial (**46b**) [59]; the ambergris odorants okoumal (**47a**) and disila-okoumal (**47b**) [60]; the woody-ambery odorant **48a** and its sila-analogues **48b–48d** [61]; the floral odorants coranol (**49a**), sila-coranol (**49b**), dimetol (**50a**), and sila-dimetol (**50b**) [62]; the musk odorant **51a** and its sila-analogues **51b–51d** [62]; the musk odorants phantolide (**52a**) and disila-phantolide (**52b**) [63]; the patchouli odorants **53a** and **53b** [64]; the musk odorant **54a** and its sila-analogues **54b–54d** [65]; the musk odorants galaxolide (**55a**) and disila-galaxolide (**55b**) [66]; and the grapefruit odorants rhubafuran (**56a**), sila-rhubafuran (**56b**) [67], methyl pamplemousse (**57a**), and sila-methyl pamplemousse (**57b**) [68].

Sila-substitution of odorants can alter and, ideally, optimize the olfactory properties by affecting the binding affinity to the olfactory receptors, which can change both the olfactory profile and the odor threshold. These are quite promising perspectives for fragrance industry, which indeed has started to use the high potential of the carbon/silicon switch strategy for odorant design and development.

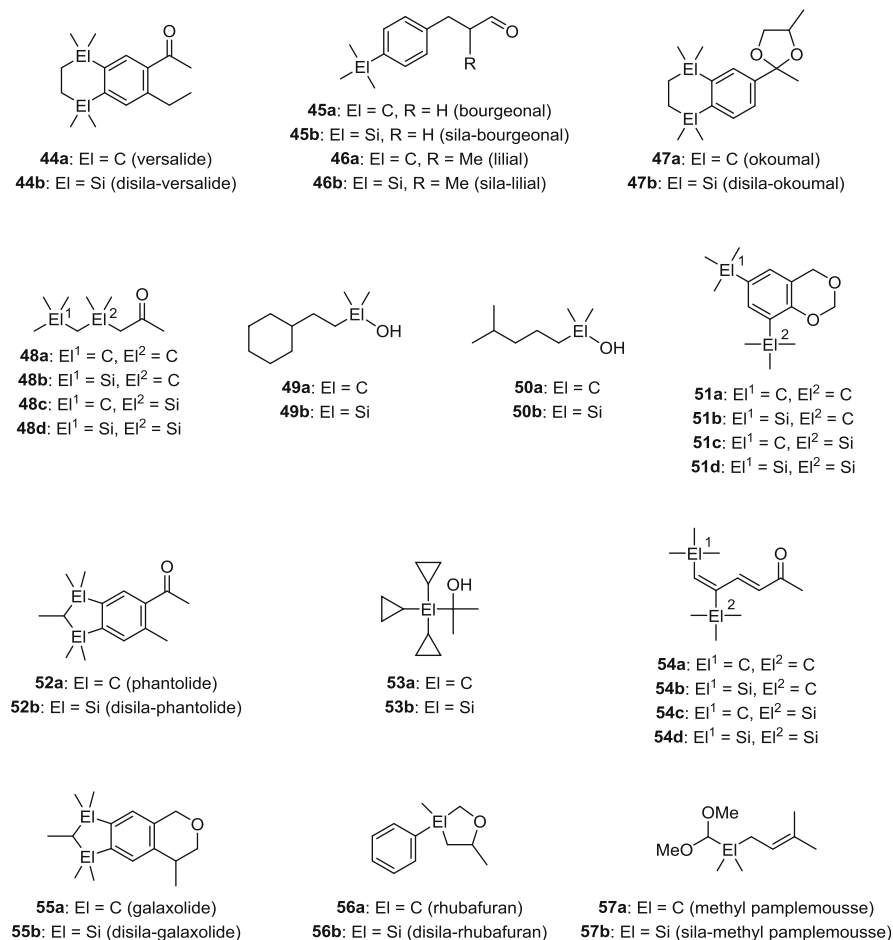


**Fig. 25** Chemical structures of the C/Si pairs **44a/44b–57a/57b**, **48a/48c**, **48a/48d**, **51a/51c**, **51a/51d**, **54a/54c**, and **54a/54d**

## 5 Summary and Outlook

Following the first pioneering studies on biologically active organosilicon compounds five decades ago, silicon chemistry is nowadays accepted to be a novel source of chemical diversity in drug design. The carbon/silicon switch strategy, i.e., the strategic replacement of a carbon atom with a silicon atom (sila-substitution) within a well-known drug, with the rest of the molecule being identical, is one of the methods that are currently used for the design and development of new silicon-based drugs. As members of Group 14 of the periodic table, the elements carbon and silicon show many similarities in their chemical properties, but there are also some fundamental differences that can lead to striking differences in the physicochemical

and biological properties of drugs and their corresponding sila-analogues. In general, the sila-analogues share the same mode of action as the parent carbon compounds (carbon/silicon bioisosterism) but may have altered biological properties. Generally, sila-substitution can affect and, ideally, improve the pharmacological potency and selectivity, the pharmacodynamics, and the pharmacokinetics. Thus, the strategic sila-substitution of existing drugs is a very promising approach for the search of new drug candidates that have beneficial properties. The carbon/silicon switch strategy is a very powerful tool for both (1) the evaluation of structure–activity relationships in basic research and (2) the development of new silicon-based drugs for clinical applications. In this context, it is important to note that up to now there are no indications for a silicon-specific toxicity associated with organosilicon compounds, in contrast to the element-associated toxicity of organogermanium, tin, and lead compounds. This lack of inherent toxicological issues with silicon and the increasing clinical experience with organosilicon compounds will stimulate the search for new silicon-based drugs for clinical applications.

When assessing the potential of the carbon/silicon switch strategy for the design and development of new silicon-based drugs, some fundamental limitations have also to be mentioned. There are chemistry-driven rules in terms of both synthetic accessibility and chemical stability that dictate whether or not and where a silicon atom can be introduced into a given drug scaffold. Synthetic organosilicon chemistry is a very rapidly developing field, and therefore, the issue “synthetic accessibility” will constantly change depending on the future developments in synthetic organosilicon chemistry, whereas the issue “chemical stability” is of course a constant factor.

The perspectives of the carbon/silicon switch strategy for pharmaceutical industry look quite promising. Generally, incorporation of silicon into a known drug can affect the pharmacological potency and selectivity, the pharmacodynamics, and the pharmacokinetics and therefore can lead to beneficial biological properties that can be used with a clear IP position. The carbon/silicon switch strategy allows to follow in the development footsteps of the already optimized parent carbon compound and thereby to speed up the development process of the sila-analogue. There is a very efficient chemical industry, with a special expertise in organosilicon chemistry, that can supply pharmaceutical industry with the silicon-based fine chemicals needed. Nowadays, the carbon/silicon switch strategy is already an established tool in drug design and development in pharmaceutical industry, and it is anticipated that this approach will play an increasingly important role in the future.

## References

1. Fessenden RJ, Fessenden JS (1967) *Adv Drug Res* 4:95
2. Voronkov MG, Lukevics E (1969) *Russ Chem Rev* 38:975
3. Garson LR, Kirchner LK (1971) *J Pharm Sci* 60:1113
4. Tacke R, Wannagat U (1979) *Top Curr Chem* 84:1

5. Voronkov MG (1979) *Top Curr Chem* 84:77
6. Tacke R, Zilch H (1986) *Endeavour. New Series* 10:191
7. Tacke R, Becker B (1987) *Main Group Met Chem* 10:169
8. Tacke R, Linoh H (1989) *Bioorganosilicon chemistry* In: Patai S, Rappoport Z (eds) *The chemistry of organic silicon compounds, part 2*. Wiley, Chichester, p 1143
9. Bains W, Tacke R (2003) *Curr Opin Drug Discovery Dev* 6:526
10. Showell GA, Mills JS (2003) *Drug Discovery Today* 8:551
11. Mills JS, Showell GA (2004) *Expert Opin Investig Drugs* 13:1149
12. Pooni PK, Showell GA (2006) *Mini-Rev Med Chem* 6:1169
13. Sieburth SMcN, Chen C-A (2006) *Eur J Org Chem* 311
14. Gately S, West R (2007) *Drug Dev Res* 68:156
15. Franz AK (2007) *Curr Opin Drug Discovery Dev* 10:654
16. Meanwell NA (2011) *J Med Chem* 54:2529
17. Franz AK, Wilson SO (2013) *J Med Chem* 56:388
18. Sieburth SMcN (2014) *Top Med Chem*. doi:[10.1007/7355\\_2014\\_80](https://doi.org/10.1007/7355_2014_80)
19. Fessenden RJ, Coon MD (1965) *J Med Chem* 8:604
20. Fessenden RJ, Ahlfors C (1967) *J Med Chem* 10:810
21. Fessenden RJ, Rittenhouse R (1968) *J Med Chem* 11:1070
22. Fessenden RJ, Hartman RA (1970) *J Med Chem* 13:52
23. Klapötke TM, Krumm B, Ilg R, Troegel D, Tacke R (2007) *J Am Chem Soc* 129:6908
24. Evangelisti C, Klapötke TM, Krumm B, Nieder A, Berger RJF, Hayes SA, Mitzel NW, Troegel D, Tacke R (2010) *Inorg Chem* 49:4865
25. Klapötke TM, Krumm B, Nieder A, Richter O, Troegel D, Tacke R (2012) *Z Anorg Allg Chem* 638:1075
26. Daiss JO, Burschka C, Mills JS, Montana JG, Showell GA, Warneck JBH, Tacke R (2006) *Organometallics* 25:1188
27. Tacke R, Daiss J (2003) *International Patent Application* WO2003 037905
28. Daiss JO, Penka M, Burschka C, Tacke R (2004) *Organometallics* 23:4987
29. Showell GA, Miller D, Mandal AK, Tacke R, Daiss J (2004) *International Patent Application* WO2004 094436
30. Showell GA, Barnes MJ, Daiss JO, Mills JS, Montana JG, Tacke R, Warneck JBH (2006) *Bioorg Med Chem Lett* 16:2555
31. Warneck JB, Cheng FHM, Barnes MJ, Mills JS, Montana JG, Naylor RJ, Ngan M-P, Wai M-K, Daiss JO, Tacke R, Rudd JA (2008) *Toxicol Appl Pharmacol* 232:369
32. Tacke R, Heinrich T, Bertermann R, Burschka C, Hamacher A, Kassack MU (2004) *Organometallics* 23:4468
33. Tacke R, Heinrich T (2003) *UK Patent Application* GB2003 2 382 575
34. Tacke R, Popp F, Müller B, Theis B, Burschka C, Hamacher A, Kassack MU, Schepmann D, Wünsch B, Jurva U, Wellner E (2008) *ChemMedChem* 3:152
35. Tacke R, Nguyen B, Burschka C, Lippert WP, Hamacher A, Urban C, Kassack MU (2010) *Organometallics* 29:1652
36. Johansson T, Weidolf L, Popp F, Tacke R, Jurva U (2010) *Drug Metab Dispos* 38:73
37. Daiss JO, Burschka C, Mills JS, Montana JG, Showell GA, Fleming I, Gaudon C, Ivanova D, Gronemeyer H, Tacke R (2005) *Organometallics* 24:3192
38. Montana JG, Showell GA, Fleming I, Tacke R, Daiss J (2004) *International Patent Application* WO2004 048390
39. Büttner MW, Nätischer JB, Burschka C, Tacke R (2007) *Organometallics* 26:4835
40. Luger P, Weber M, Hübschle C, Tacke R (2013) *Org Biomol Chem* 11:2348
41. Lippert WP, Burschka C, Götz K, Kaupp M, Ivanova D, Gaudon C, Sato Y, Antony P, Rochel N, Moras D, Gronemeyer H, Tacke R (2009) *ChemMedChem* 4:1143
42. Bauer JB, Lippert WP, Dörrich S, Tebbe D, Burschka C, Christie VB, Tams DM, Henderson AP, Murray BA, Marder TB, Przyborski SA, Tacke R (2011) *ChemMedChem* 6:1509

43. Büttner MW, Burschka C, Daiss JO, Ivanova D, Rochel N, Kammerer S, Peluso-Iltis C, Bindler A, Gaudon C, Germain P, Moras D, Gronemeyer H, Tacke R (2007) *ChemBioChem* 8:1688
44. Tacke R, Müller V, Büttner MW, Lippert WP, Bertermann R, Daiß JO, Khanwalkar H, Furst A, Gaudon C, Gronemeyer H (2009) *ChemMedChem* 4:1797
45. Gluyas JBG, Burschka C, Dörrich S, Vallet J, Gronemeyer H, Tacke R (2012) *Org Biomol Chem* 10:6914
46. Tacke R, Kornek T, Heinrich T, Burschka C, Penka M, Pülm M, Keim C, Mutschler E, Lambrecht G (2001) *J Organomet Chem* 640:140
47. Tacke R, Handmann VI, Kreutzmann K, Keim C, Mutschler E, Lambrecht G (2002) *Organometallics* 21:3727
48. Tacke R, Handmann VI, Bertermann R, Burschka C, Penka M, Seyfried C (2003) *Organometallics* 22:916
49. Heinrich T, Buschka C, Warneck J, Tacke R (2004) *Organometallics* 23:361
50. Tacke R, Schmid T, Penka M, Burschka C, Bains W, Warneck J (2004) *Organometallics* 23:4915
51. Ilg R, Burschka C, Schepmann D, Wünsch B, Tacke R (2006) *Organometallics* 25:5396
52. Barnes MJ, Burschka C, Büttner MW, Conroy R, Daiss JO, Gray IC, Hendrick AG, Tam LH, Kuehn D, Miller DJ, Mills JS, Mitchell P, Montana JG, Muniandy PA, Rapley H, Showell GA, Tebbe D, Tacke R, Warneck JBH, Zhu B (2011) *ChemMedChem* 6:2070
53. Wang J, Ma C, Wu Y, Lamb RA, Pinto LH, DeGrado WF (2011) *J Am Chem Soc* 133:13844
54. Reddy GD, Park S-J, Cho HM, Kim T-J, Lee ME (2012) *J Med Chem* 55:6438
55. Tacke R, Bertermann R, Burschka C, Dörrich S, Fischer M, Müller B, Meyerhans G, Schepmann D, Wünsch B, Arnason I, Björnsson R (2012) *ChemMedChem* 7:523
56. Fujii S, Miyajima Y, Masuno H, Kagechika H (2013) *J Med Chem* 56:160
57. Nakamura M, Makishima M, Hashimoto Y (2013) *Bioorg Med Chem* 21:1643
58. Büttner MW, Penka M, Doszczak L, Kraft P, Tacke R (2007) *Organometallics* 26:1295
59. Doszczak L, Kraft P, Weber H-P, Bertermann R, Triller A, Hatt H, Tacke R (2007) *Angew Chem* 119:3431; (2007) *Angew Chem Int Ed* 46:3367
60. Büttner MW, Burschka C, Junold K, Kraft P, Tacke R (2007) *ChemBioChem* 8:1447
61. Büttner MW, Metz S, Kraft P, Tacke R (2007) *Organometallics* 26:3925
62. Tacke R, Metz S (2008) *Chem Biodiversity* 5:920
63. Metz S, Nätscher JB, Burschka C, Götz K, Kaupp M, Kraft P, Tacke R (2009) *Organometallics* 28:4700
64. Sunderkötter A, Lorenzen S, Tacke R, Kraft P (2010) *Chem Eur J* 16:7404
65. Geyer M, Bauer J, Burschka C, Kraft P, Tacke R (2011) *Eur J Inorg Chem* 2769
66. Dörrich S, Bauer JB, Lorenzen S, Mahler C, Schweetberg S, Burschka C, Baus JA, Tacke R, Kraft P (2013) *Chem Eur J* 19:11396
67. Förster B, Bertermann R, Kraft P, Tacke R (2014) *Organometallics* 33:338
68. Friedrich J, Dörrich S, Berkefeld A, Kraft P, Tacke R (2014) *Organometallics* 33:796

Atypical Elements in Drug Design

Schwarz, J. (Ed.)

2016, VII, 158 p. 90 illus., 18 illus. in color., Hardcover

ISBN: 978-3-319-27740-0